

## Article

# Numerical Study on Heat Transfer Efficiency of Regenerative Thermal Oxidizers with Three Canisters

Guangyi Pu <sup>1,2</sup>, Xiaoyin Li <sup>1,2</sup> and Fangyang Yuan <sup>1,2,\*</sup>

<sup>1</sup> Jiangsu Key Laboratory of Advanced Food Manufacturing Equipment and Technology, Jiangnan University, Wuxi 214122, China; puguangyi@jiangnan.edu.cn (G.P.); 6200809017@stu.jiangnan.edu.cn (X.L.)

<sup>2</sup> School of Mechanical Engineering, Jiangnan University, Wuxi 214122, China

\* Correspondence: fyyuan@jiangnan.edu.cn

**Abstract:** The heat transfer efficiency of a regenerative thermal oxidizer with three canisters used for volatile organic compounds treatment was studied using numerical simulation methods. A one-dimensional model that took into account the variation of physical parameters with temperature was built. The results show that the preheating temperature and outlet temperature tend to be stable as the operation time is increased. The heat transfer efficiency of equipment was mainly evaluated by heat recovery efficiency and energy recovery ratio under steady state conditions, which was affected by the inlet gas flow and temperature, valve switch time, combustion temperature, materials and porosity of the regenerative medium, and packing height. With the increase in packing cross-sectional area and packing height, the increase in heat transfer efficiency leads to an increase in equipment cost. Simultaneously, the shorter the valve switch time and the higher the density of the regenerative medium battery also help to improve the heat transfer efficiency without blocking equipment. Unless the removal efficiency of volatile organic compound treatment is reduced, it is recommended to reduce the inlet and combustion temperatures.



**Citation:** Pu, G.; Li, X.; Yuan, F. Numerical Study on Heat Transfer Efficiency of Regenerative Thermal Oxidizers with Three Canisters. *Processes* **2021**, *9*, 1621. <https://doi.org/10.3390/pr9091621>

Academic Editor: Kody Powell

Received: 3 August 2021

Accepted: 7 September 2021

Published: 8 September 2021

**Publisher's Note:** MDPI stays neutral with regard to jurisdictional claims in published maps and institutional affiliations.



**Copyright:** © 2021 by the authors. Licensee MDPI, Basel, Switzerland. This article is an open access article distributed under the terms and conditions of the Creative Commons Attribution (CC BY) license (<https://creativecommons.org/licenses/by/4.0/>).

**Keywords:** regenerative thermal oxidizer; honeycomb ceramic regenerator; thermal recovery efficiency; energy recovery ratio

## 1. Introduction

Reducing the intensity of energy consumption intensity and total emissions of major pollutants has become China's economic development constraint. The government has pledged to cap carbon dioxide emissions by 2030 and achieve carbon neutrality by 2060. The volatile organic compounds (VOC) emitted into the environment accounted for one-third of the total pollutant emissions in industry. The direct emission of organic waste gases will not only cause environmental pollution such as haze and photochemical haze, but also be extremely toxic to humans. High temperature air combustion (HTAC) [1] is one of the most effective industrial technologies for VOC treatment because it can oxidize volatile organic compounds under high temperatures into allowable emissions of gases. However, the disadvantages are high energy consumption and high treatment costs. Therefore, a regenerative thermal oxidizer (RTO) [2] is developed to collect the heat energy from the air, resulting in efficient treatment of volatile organic compounds, energy savings and environmental protection.

The RTO is a regenerator that exchanges heat with the VOC-containing gas using a large number of regenerative media with high heat capacity. The heat exchanger is to heat the inlet low temperature gas by recovering the energy from the outlet high temperature gas. This exchange process is unsteady, and combines fluid flow and heat transfer. Periodic heat transfer is achieved by opening or closing the switching valves. Because the RTO with two regenerators produces exhaust gas escape during valve switching and increases the exhaust concentration in an instantaneous state, the RTO with three canisters is the most widely used regenerator in industry. The addition of a purging configuration in the

regenerator balances the efficiency and economic requirements of treatment [3,4], which is suitable for VOC treatment with a flow rate of  $10,000\sim 40,000\text{ m}^3\cdot\text{h}^{-1}$ , and the VOC removal rate is usually more than 98%. The main purpose of the RTO system design is to save energy consumption on the premise of ensuring clear efficiency. In other words, improving the heat recovery efficiency is one of the key properties of the RTO. On the one hand, due to the operation of the equipment in the high-temperature range, it is important to achieve thermal insulation efficiently. On the other hand, it is necessary to design process parameters and equipment structure reasonably to ensure an efficient heat transfer process.

Although RTO has been studied for decades, the related research has not ceased in recent years. The latest literature on important research is summarized in Table 1. Kang et al. [5,6] conducted an experimental study on the thermal efficiency of a regenerator system for a combustion furnace. They found that about 40% of exhaust gas was required to prevent the saturation of porous regenerative media, resulting in the effective utilization of exhaust heat. Gosiewski et al. [7,8] simulated the flow and energy recovery processes in reverse-flow reactors with two sections. The computational fluid dynamics (CFD) method has been validated for use in industry. They discussed the flow uniformity in the reactors and found a lack of uniformity at the top of the channel due to high velocity. Lin et al. [9] numerically investigated the thermal-hydraulic properties of a packed bed regenerator. The results revealed that the spanwise heat transfer coefficient changed in the opposite direction during the heating and regeneration period. Marin et al. [10,11] analyzed an RTO used for methane gas reduction during coal mining and concluded that the proposed feedback control system could regulate the heat storage system, to keep the temperature of each component constant. A three-dimensional model was built by You et al. [12] to simulate the coupled heat transfer of honeycomb packing heat exchangers with small square channels. It was found that the heat recovery efficiency increased with the increase in packing height. Furthermore, they presented the heat transfer and flow resistance performances of the RTOs with the parallel or crosswise arrangement of circular holes, and found the optimal lengths of these arrangements are approximately 307 mm and 342 mm, respectively [13]. Yuan et al. [14] compared regenerative media with square openings and hexagon openings finding that the energy recovery ratio of regenerative media with the square openings was 5% to 16% higher than that of hexagon opening regenerative media, while the pressure loss increased with the decreasing of opening side length. Alfarawi et al. [15] showed combined research based on experiments and the CFD approach, discussing the heat transfer and resistance characteristics of mini-channel RTOs with different channel hydraulic diameters. The results revealed that the heat transfer coefficient increased with the decrease of opening length, followed by an increase in pressure drop. Lan and Li [16] conducted a 3D simulation and found that the cycle for the steady-state was symmetrical. The minimum feed gas concentration of self-sustaining operation increased significantly with decreasing channel length and increasing inlet velocity and was nearly independent of cycle time. Hao et al. [3,17] discussed key factors in the VOCs treatment by RTO with three canisters. There was a backflushing process during operation and different parameters imposed various influences on key factors, such as the oxidation chamber temperature (OCT), outlet temperature, and thermal efficiency. Gao et al. [18] carried out experiments on the thermal oxidation of methane in a thermal reverse flow reactor and found that the system could run automatically under a wide range of operating conditions and achieved high methane conversion. The methane conversion was affected by the inlet concentration instead of the inlet flow rate. A wavelet optimized finite difference method (FDM) was developed to simulate the thermal regenerator by Singh et al. [19] and Kumar and Murthy [20]. The method helped to produce an adaptive grid scheme that can improve calculation accuracy and reduce time-consuming. The analysis of how different inlet-outlet-purge configurations affect the efficiency of VOC removal done by Giuntini et al. [4] showed that the removal efficiency of VOCs was the lowest when the central canister was the outlet. The authors also suggested that strict criteria should be established for RTO intensification.

**Table 1.** Comparison of recent regenerative thermal oxidizer (RTO) studies (listed in chronological order).

Authors	Year	Method of Research	Number of Canisters	Material/Dimension of Filler	Valve Switch Time (s)	Thermal Efficiency
Kang et al. [5,6]	2014, 2015	Numerical & Experimental	2	$D = 70$ mm, 35 mm $L = 100, 50, 25, 13$ mm	30~900	>72%
Lin et al. [9]	2016	Experimental	5	-	-	-
Marin et al. [10,11]	2014, 2020	Numerical	3	Refractory ceramics	120	Up to 99%
You et al. [13,21]	2016, 2019	Numerical	2	Square/ceramic	15~90	-
Yuan et al. [14]	2017	Numerical	2	Cordierite-mullite Square/hexagon	20~40	50~82%
Alfarawi et al. [15]	2017	Numerical& Experimental	1	$D = 1.5, 1, 0.5$ mm	-	-
Lan and Li [16]	2018	Numerical	1	Square	-	-
Hao et al. [3,17]	2018, 2020	Numerical& Experimental	3	Square	-	>75%
Gao et al. [18]	2019	Experimental	1	Square/ceramic	60~120	-
Giuntini et al. [4]	2020	Numerical	3	ceramic	90	-

To summarize, the heat transfer performance of RTO has been studied extensively. However, there have been few studies on the heat transfer performance of a three-canister RTO that includes three stages of the inlet, outlet and purge all at the same time. Considering the RTO has been widely applied in industry, it is important to evaluate the change in heat transfer performance of the three-canister RTO with key parameters. The purpose of this paper is to investigate the impact of structure and operation parameters on RTO's high heat recovery efficiency.

## 2. Physical Model

Figure 1 and Table 2 show the schematic diagram and specifications of a 3-canister RTO, respectively. It is fixed equipment that runs on-site to remove the VOCs in a paper mucilage glue company in China, and it consists of a combustion chamber with two burners, three heat storage modules filled with honeycomb ceramic media, supporting plates and concrete slabs, air distribution chambers and a stand, inlet pipes and purge pipes, switching valves, etc. Convection heat transfer occurs when gas flows through the surface of the heat storage medium. Heat can be transferred from the hot fluid after HTAC to the cold fluid by the periodic flow on the solid surface. Heat loss occurs during this process, so it is necessary to introduce burners to maintain the temperature of the combustion chamber and to increase the air distributor to keep the uniformity of gas temperature. Unlike the RTO with two canisters, it followed the inlet configuration at the switch of the purge process; subsequently, the untreated gases that remained in the chamber are pushed into the combustion chamber, thus avoiding the increase in VOCs concentration in the outlet.

**Table 2.** Specifications of the RTO.

Parameters	Value	Parameters	Value
Total height	7581 mm	Total length	12,214 mm
Combustion chamber height	1975 mm	Total width	2264 mm
Packing height	1600 mm	Canister length	3080 mm
Insulating layer thickness	250 mm	Canister width	2310 mm

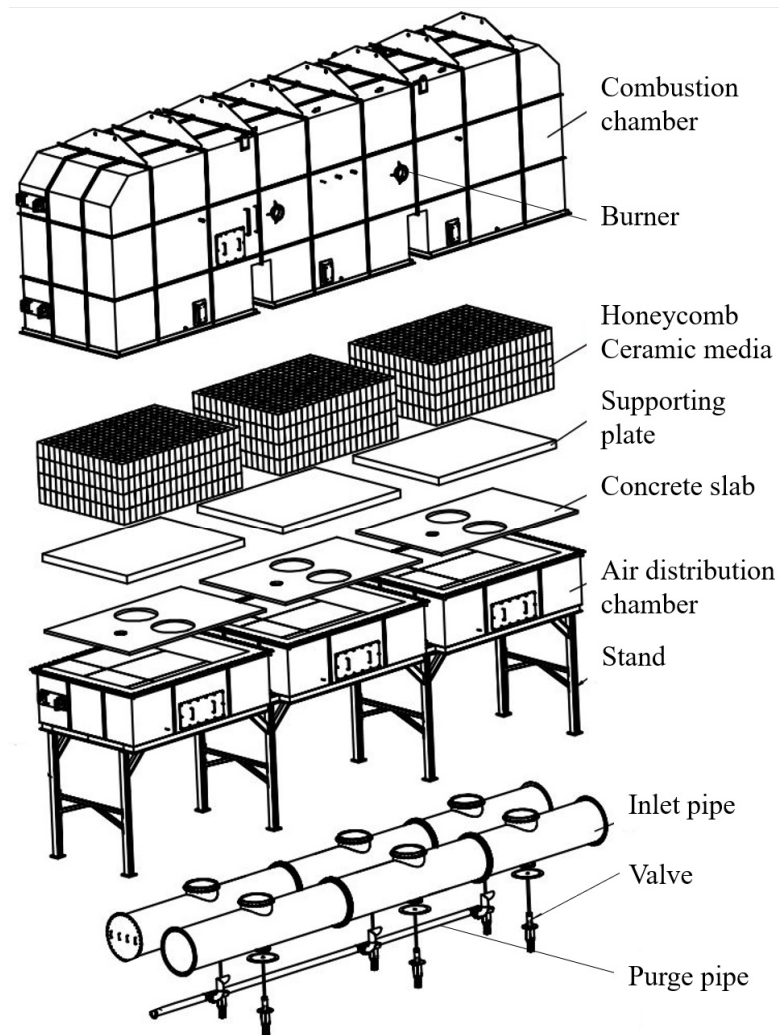


**Figure 1.** Structure of a three-canister RTO.

Figure 2 shows the working circulation of a three-canister RTO with three states of A, B, and C. Each regenerator goes through three processes: inlet preheating, outlet exhaust heat release, and purging via the switch of the valve. Taking the operation form of the left canister as an example, it is clear that the operation form of a single canister is shown in Figure 3. As time passes, the single chamber gas-solid coupled heat transfer accumulates three valve intervals as a total cycle. The working cycle of the regenerator will enter a stable state regardless of the initial temperature of the regenerator, as long as there is a sufficient heat transfer cycle. That is, the temperature changes between cycles are usually consistent.

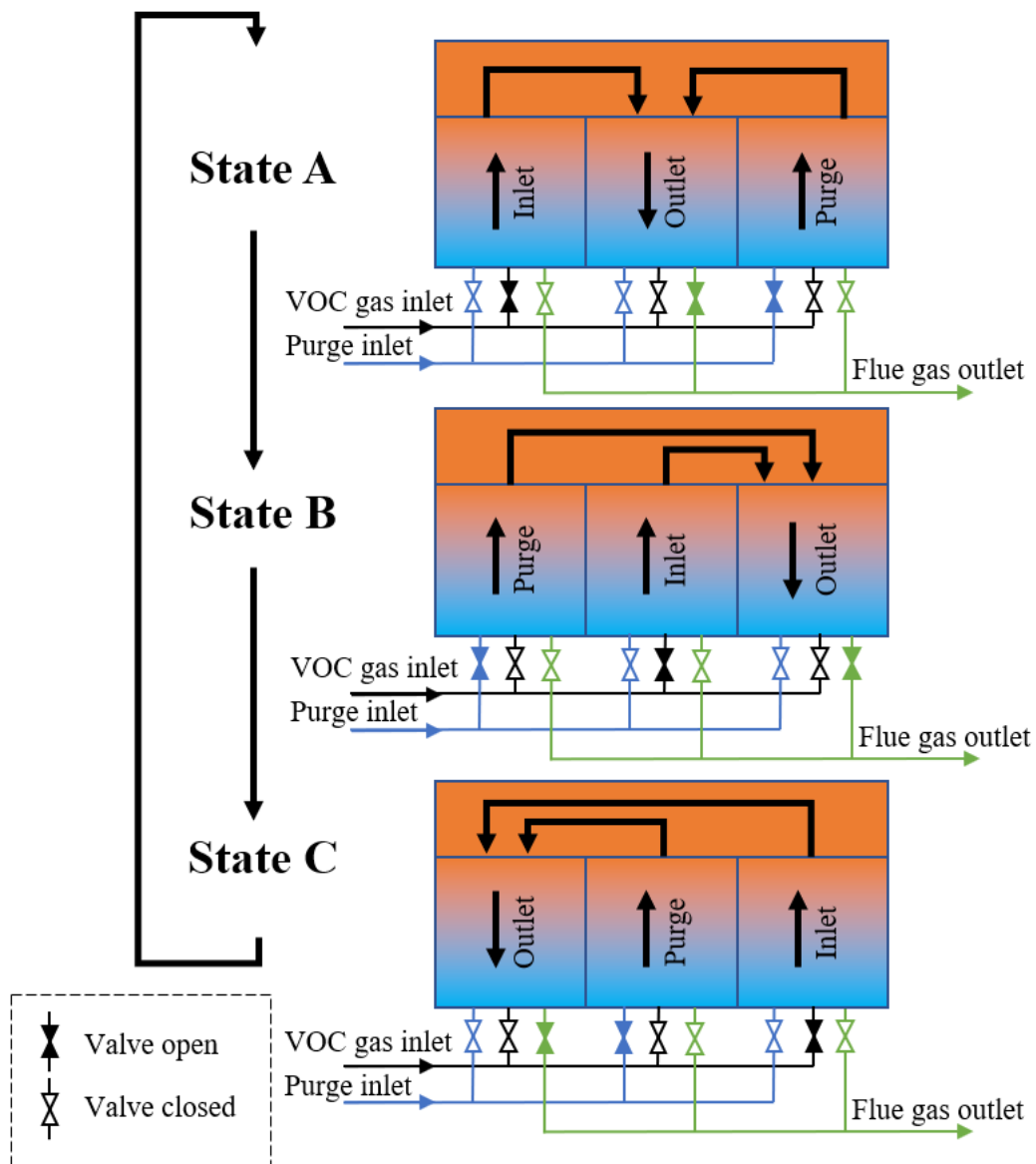


Figure 2. Working circulations of the regenerator with three states (VOC refers to volatile organic compounds).

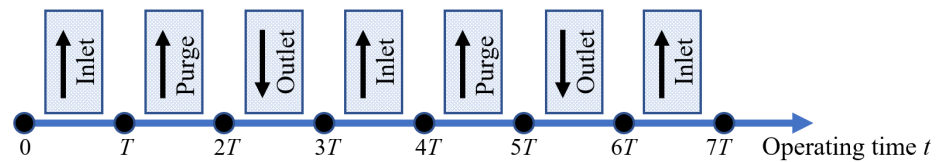


Figure 3. Operating profile of a certain canister (where  $T$  is the valve switch time).

### 3. Numerical Methods

#### 3.1. Governing Equations

The governing equations for the gas flow in the regenerator are the continuity equation, Navier–Stokes equation, and the energy conservation equation [22]:

$$\frac{\partial \rho_g}{\partial t} + \nabla \cdot (\rho_g \mathbf{u}) = 0 \tag{1}$$

$$\frac{\partial}{\partial t} (\rho_g \mathbf{u}) + \nabla \cdot (\rho_g \mathbf{u} \mathbf{u}) = \rho_g \mathbf{g} - \nabla p + \mu \nabla^2 \mathbf{u} \tag{2}$$

$$\frac{\partial}{\partial t}(\rho_g T_g) + \nabla \cdot (\mathbf{u} \rho_g T_g) = \nabla \cdot (k_g \nabla T_g) \quad (3)$$

where  $\mathbf{u}$ ,  $p$ ,  $\rho_g$ ,  $\mathbf{g}$ , and  $\mu$  are the velocity, pressure, gas density, gravitational body force, and viscosity, respectively.  $T_g$ , and  $k_g$  are the gas temperature and thermal conductivity, respectively.

The energy transport equation in solid regions is:

$$\frac{\partial}{\partial t}(\rho_s h_s) + \nabla \cdot (\mathbf{u} \rho_s h_s) = \nabla \cdot (k_s \nabla T_s) \quad (4)$$

where  $h_s$ ,  $k_s$ ,  $T_s$  are the solid enthalpy, thermal conductivity, and temperature, respectively.

### 3.2. Computation Domain and Mesh Generation

Stacking hexahedral honeycomb ceramic modules were used to create the regenerator packing. To simplify the model, the heat transfer process of the regenerator was assumed to be as follows: (a) the fluid flowing in the regenerator is incompressible ideal gas; (b) the gas flow and heat transfer in each channel of the regenerator are the same, a single channel can be selected for calculation; (c) the thermal physical parameters of the fluid and heat storage medium vary with temperature; (d) ignore the chemical reactions of flue gas in the internal of the regenerator.

Because the distribution of the regenerator inner holes is periodic and the flow parameters inside the regenerator are symmetrical, so 1/4 of the circulating unit of the regenerator was chosen as the calculation domain. Therefore, the three-dimensional region composed of the 1/4 section of the circulation chamber and the whole regenerator length direction is shown in Figure 4. The computational region was discretized using hexahedral structured grids that were refined near the wall. The mesh dependency test was performed and the grid system consisting of  $9(X) \times 12(Y) \times 1400(Z) = 151,200$  nodes was chosen for simulations, as seen in Table 3. A similar mesh generation strategy was adopted for the other type of RTO with different dimensions mentioned below.

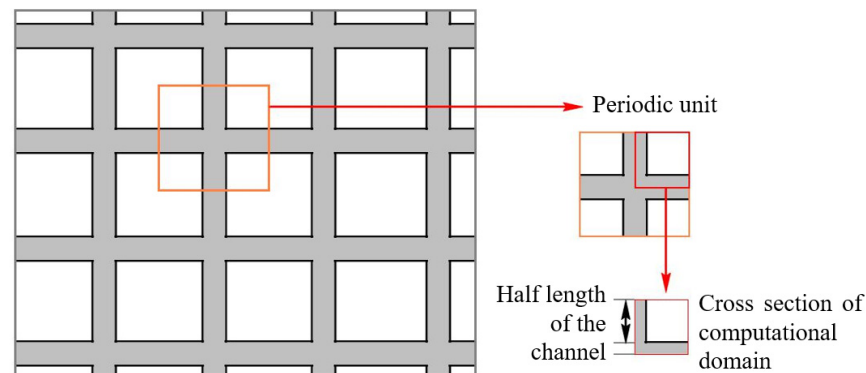


**Figure 4.** Simplification of the calculation model of the regenerator.

**Table 3.** Mesh independency test.

Mesh Name	Number of Elements (X × Y × Z)	Outlet Gas Temperature (°C)
Mesh 1	6 × 9 × 1200	82.39
Mesh 2	9 × 12 × 1400	79.85
Mesh 3	15 × 20 × 2000	79.78

### 3.3. Parameters and Physical Models

The temperature range of gas flow in the regenerator is very wide, resulting in a great influence of temperature on the physical properties of gas and solids. Therefore, accurate models are required to characterize the physical properties of materials. Dense alumina with a density of  $2600 \text{ kg}\cdot\text{m}^{-3}$  was used as the regeneration medium. It is

widely assumed that the specific heat capacity and thermal conductivity of the regenerator change linearly with temperature, ranging from 900 ( $\text{J}\cdot\text{kg}^{-1}\cdot\text{°C}^{-1}$ ) to 1100 ( $\text{J}\cdot\text{kg}^{-1}\cdot\text{°C}^{-1}$ ) and 1.5 ( $\text{W}\cdot\text{m}^{-1}\cdot\text{K}^{-1}$ ) to 3 ( $\text{W}\cdot\text{m}^{-1}\cdot\text{K}^{-1}$ ) when temperatures range from 20 °C to 1000 °C, respectively). Table 4 gives the thermal properties of air parameters which were obtained by fitting the standard values from handbook [23] with polynomial expressions. The gas mixture containing VOC was obtained by mixing theory. The density, specific heat capacity, and thermal conductivity of the gas were calculated by the polynomial model, and the viscosity was described by the Sutherland model with three parameters. The relative error was within 2.2% of the exact values.

**Table 4.** Thermal properties of air parameters.

Parameters	Model	Error
Density $\rho$ , $\text{kg}\cdot\text{m}^{-3}$	polynomial: $4.06049 - 0.01857 \times T + 4.32309 \times 10^{-5} \times T^2 - 5.41625 \times 10^{-8} \times T^3 + 3.47066 \times 10^{-11} \times T^4 - 8.913 \times 10^{-15} \times T^5$	<1%
Heat capacity $C_p$ , $\text{J}\cdot\text{kg}^{-1}\cdot\text{°C}^{-1}$	polynomial: $1161.482 - 2.368819 \times T + 0.01485511 \times T^2 - 5.034909 \times 10^{-5} \times T^3 + 9.928569 \times 10^{-8} \times T^4 - 1.111 \times 10^{-10} \times T^5 + 6.54 \times 10^{-14} \times T^6 - 1.573588 \times 10^{-17} \times T^7$	<0.28%
Heat conductivity $k$ , $\text{W}\cdot\text{m}^{-1}\cdot\text{K}^{-1}$	polynomial: $0.00582 + 5.25622 \times 10^{-5} \times T + 8.96182 \times 10^{-8} \times T^2 - 1.34213 \times 10^{-10} \times T^3 + 5.4461 \times 10^{-14} \times T^4$	<0.34%
Viscosity $\mu$ , $\text{kg}\cdot\text{m}^{-1}\cdot\text{s}^{-1}$	Sutherland model (three parameters): $\mu_0(T/T_0)^{1.5}(T_0 + 110.56)/(T + 100.56)$ (where $T_0$ and $\mu_0$ are reference temperature and reference viscosity, respectively)	<2.2%

### 3.4. Initial and Boundary Conditions

The setting of boundary conditions at the channel inlet and outlet needs to be changed according to the inlet-outlet-purge configurations, as can be seen in Table 5.

**Table 5.** Boundary conditions of flow channel inlet and outlet.

Configurations	Function	Packing Top	Packing Bottom
A-Inlet	Preheating	$Q_m = 2.5 \times 10^{-5} \text{ kg}\cdot\text{s}^{-1}$ $T = 800 \text{ °C}$	Pressure outlet $P = 0 \text{ Pa}$
B-Purge	Purge	Pressure outlet $P = 0 \text{ Pa}$	$Q_m = 1 \times 10^{-6} \text{ kg}\cdot\text{s}^{-1}$ $T = 65 \text{ °C}$
C-Outlet	Heat recovery	Pressure outlet $P = 0 \text{ Pa}$	$Q_m = 2.25 \times 10^{-5} \text{ kg}\cdot\text{s}^{-1}$ $T = 65 \text{ °C}$

### 3.5. Discrete Scheme and Algorithm

Parallel numerical simulations were carried out based on ANSYS Fluent 17. The incompressible unsteady algorithm was used. The second-order scheme was adopted for the pressure term in Equations (1)–(3) and second-order upwind schemes were used for momentum and energy terms. The unsteady term adopted the first-order implicit scheme. The time step was set to 0.5 s. The parameters for the benchmark case are listed in Table 6, where N represents the standard state (0 °C, 1 atm).

**Table 6.** Parameters of the benchmark case.

Parameters	Value	Parameters	Value
Valve switch time	120 s	Inlet flow rate	40,000 $\text{Nm}^3/\text{h}$
Combustion temperature	800 °C	Number of filling openings	40 × 40
Inlet air temperature	65 °C	Packing height	1.6 m

## 4. Results and Discussion

### 4.1. Calculation Verification

The operation of RTO includes three stages, that is starting stage, stable stage, and ending stage. The temperature profile of preheated gas and exhaust gas in a stable cycle is a key operating parameter for RTO. To achieve a stable state quickly, the initial temperature of the regenerative media was set at 550 K. Figure 5 shows the evolution of preheated and outlet air temperatures as a function of operating time. The interval of the vertical dotted line indicates that the equipment has completed a full working cycle. In the figure, there is a stable cycle in which the temperature of preheated and outlet gas gradually tends to be stable as the equipment operation time increases.

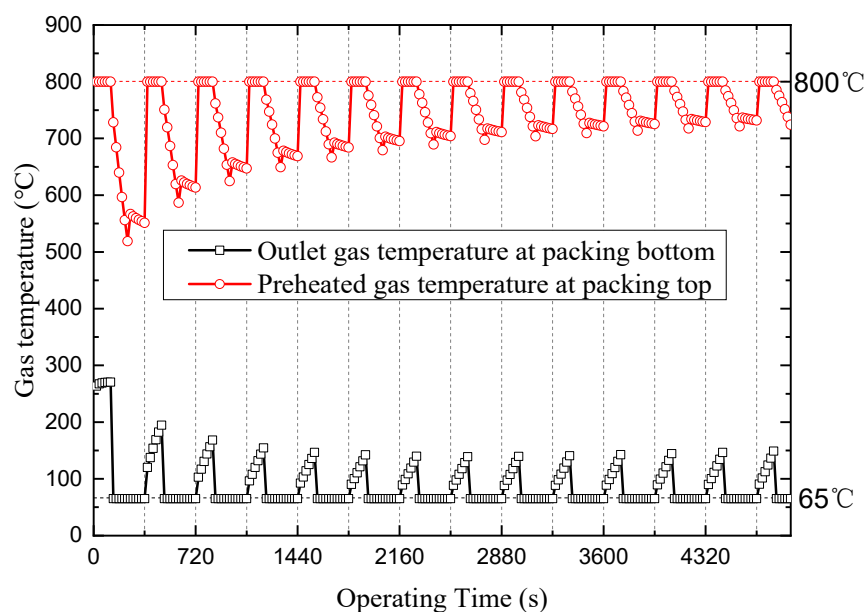


Figure 5. Temperature evolution of inlet and outlet gas temperatures.

Figure 6 shows the temperature changes of preheated and outlet gases during the stable cycle, and the experimental test data given by the company are denoted by solid dots and solid square dots. Key parameters are shown in Table 6. When the numerical calculation results were compared to the experimental data, it was found that the results are consistent, proving the effectiveness of the numerical calculation method used in this paper. The gas temperatures are changing in a similar way. That is, the outlet flue gas temperature gradually increases and the preheating air temperature gradually decreases in a single cycle. The numerical simulation results decreased rapidly when compared to the experimental data, while the outlet flue gas temperature increased slowly. Pollutant combustion in the regenerator could be the source of the relative error.

### 4.2. Temperature Distribution along with the Canister Height

Figure 7 shows the changes of gas and solid temperature with filler height in a steady state. The profile was created using the parameters listed in Table 6. At the end of the solid exothermic stage, the gas temperature and solid temperatures gradually decrease from the combustion temperature (800 °C) to 120 °C. At the end of the solid heat storage stage, the temperature of the gas and solid gradually increases from the inlet temperature (65 °C) along the height direction. Because of the low gas flow rate, the gas-solid curves almost coincide during the purge stage. According to the spatial distribution of temperature, the temperature increases with the increase in height, so the height of filler has a great influence on the preheating temperature of the gas.

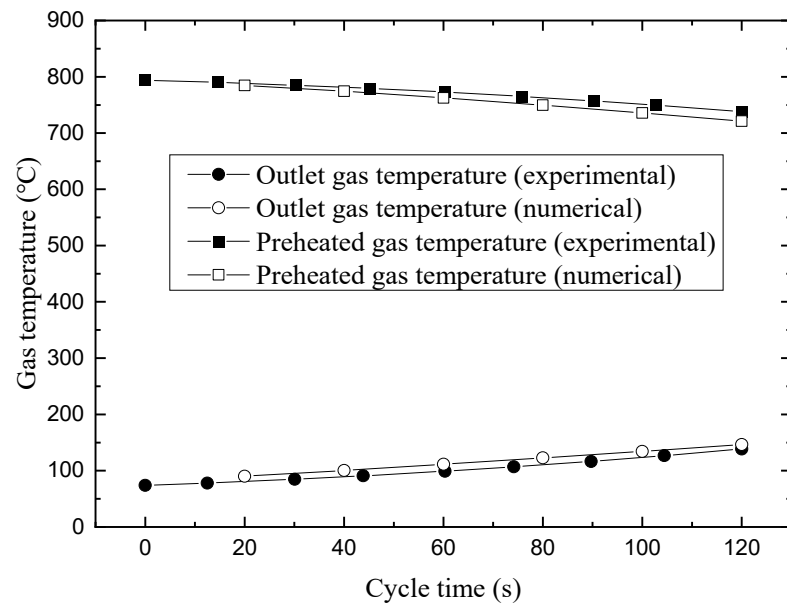


Figure 6. The temperature profile of preheated and outlet gas in a stable cycle.

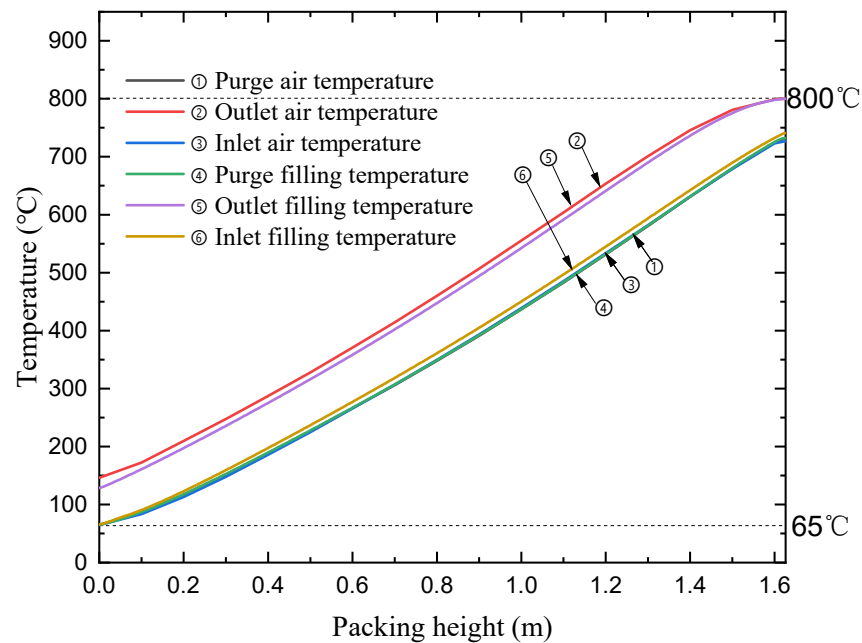


Figure 7. The temperature profile of gases and fillings along with height in a stable cycle.

#### 4.3. Thermal Efficiencies

The heat transfer efficiencies of RTO equipment used in a pulp adhesive company were numerically simulated using the above model, and the influence of key parameters on heat transfer performance was analyzed to guide the optimization design of equipment in the paper. The thermal efficiency of an RTO operating at a steady state is defined as the ratio of preheating energy supplied by the heat exchange media, and can be represented by the energy recovery ratio (ERR) [12]:

$$ERR = \frac{m_a (C_{p,h} T_{a,h} - C_{p,c} T_{a,c})}{m_g (C_{p,g} T_{g,h} - C_{p,0} T_0)} \times 100\% \quad (5)$$

where  $m$ ,  $C_p$ , and  $T$  represent the mass flow rate, specific heat, and gas temperature, respectively. The subscripts  $h$  and  $c$  indicate the hot and cold ends, and the subscripts  $a$  and  $g$  represent air and exhaust, respectively. The subscript 0 represents the room temperature environment. If the air feeding to the combustion chamber is ignored, the heat transfer performance of the RTO can also be evaluated by heat recovery efficiency ( $TRE$ ) [17]:

$$TRE = \frac{T_{a,h} - T_{g,c}}{T_{g,h} - T_{a,c}} \times 100\% \quad (6)$$

The ERR characterizes total thermal recovery. The  $TRE$  gives a simple expression and has been adopted in local technical specifications for industrial VOC treatment by RTO in 2020. Hence, both of them were shown and discussed in this section. In this paper, the effects of structure and operating parameters on the heat efficiency of RTO were discussed one by one using the control variable method.

#### 4.3.1. Effect of Inlet Flow Rate and Valve Switch Time

Figures 8 and 9 show the influence of inlet flow and valve switch time on the heat transfer efficiencies. Other parameters are set according to Table 6. The change in inlet flow rate has little effect on  $TRE$ . With the increase in flow rate,  $ERR$  increases slightly at first and then decreases, indicating that when the inlet flow rate is too high, the air flow area of the filler section should be increased to ensure that the energy recovery efficiency reaches the maximum under the appropriate processing capacity. The change of outlet gas temperature with inlet flow rate was added at the right-Y axis in Figure 8. The outlet gas temperature decreases slightly at first and then increases significantly, which shows an opposite trend to the  $ERR$  curve. Considering that the outlet gas temperature cannot be too high, the inlet flow rate for a certain RTO equipment should be controlled within a range. Figure 9 shows that if the valve switch time becomes longer,  $TRE$  and  $ERR$  decrease sharply. Furthermore, the decline of efficiencies has accelerated in the long switch time region, which is consistent with the conclusions of [5,6,12,14]. To ensure high efficiency, the valve switch time cannot be too long.

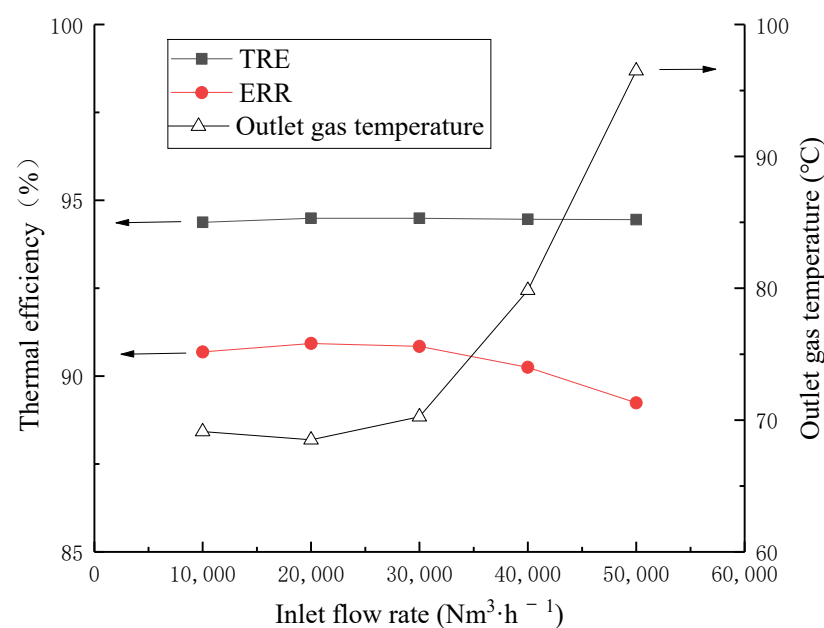


Figure 8. Effect of inlet flow rate on heat transfer efficiencies.

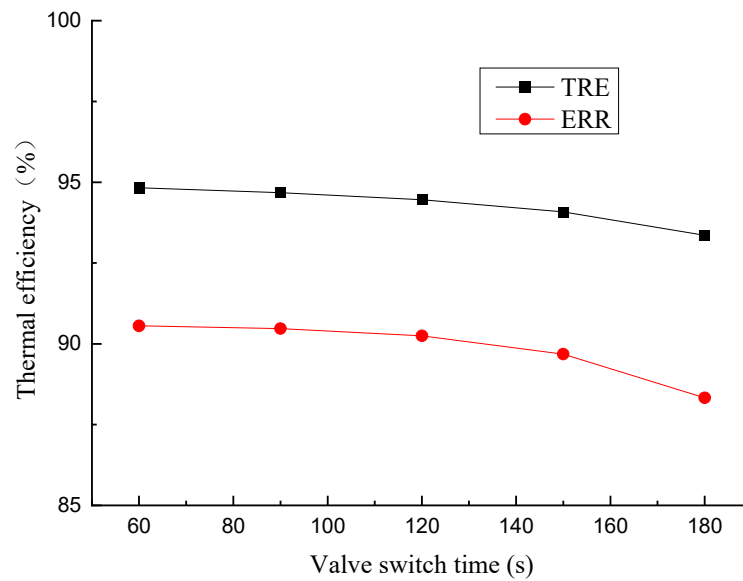


Figure 9. Effect of valve switch time on heat transfer efficiencies.

#### 4.3.2. Effect of Inlet Air Temperature and Combustion Temperature

Figures 10 and 11 show the influence of inlet air temperature and combustion temperature on heat transfer efficiencies. Other parameters are set according to Table 6. It is found that with the increase in inlet air temperature, the ERR of the RTO decreases slightly, and the heat recovery efficiency decreases significantly. The combustion temperature also has a significant impact on heat transfer efficiency, particularly when the combustion temperature exceeds 850 °C. Therefore, the temperature should not be too high when designing VOC high-temperature catalytic combustion conditions. However, in order to avoid reducing the removal efficiency of VOC, the combustion chamber temperature cannot be reduced.

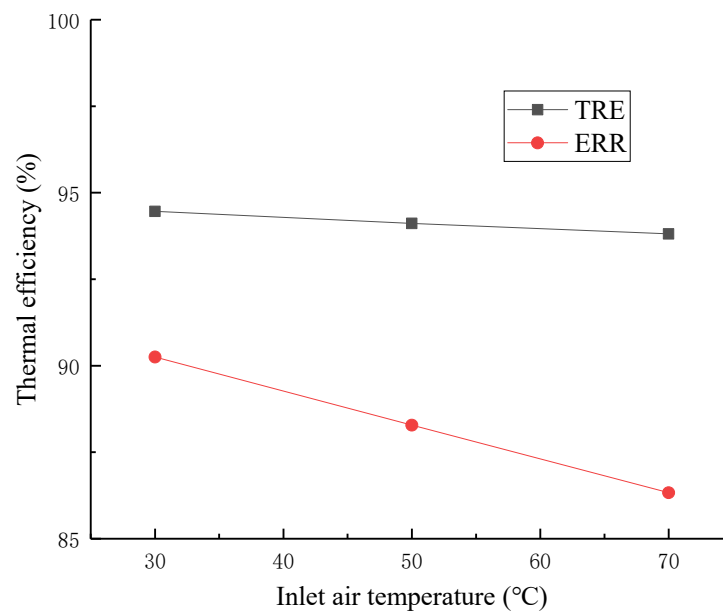
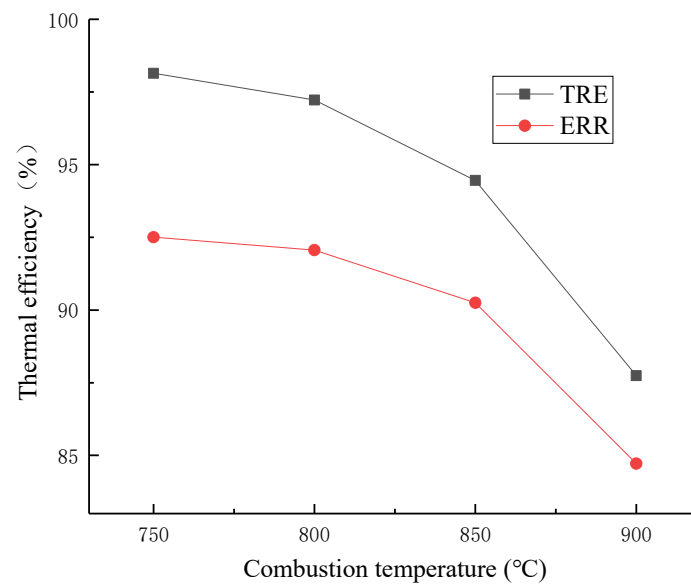


Figure 10. Effect of inlet air temperature on heat transfer efficiencies.



**Figure 11.** Effect of combustion temperature on heat transfer efficiencies.

#### 4.3.3. Effect of Regenerative Media Porosity and Packing Height

Figure 12 shows the effect of the numbers of regenerative media channels on heat transfer efficiencies. In this paper, the regeneration media with various numbers of channels under the same size filler was selected for calculation and comparison, including  $25 \times 25$ ,  $40 \times 40$ ,  $50 \times 50$ ,  $60 \times 60$  as four common pore number densities. The regenerative media porosity refers to the ratio of gas channel area to total area, and decreases with the number of regenerative module channels. The results show that the TRE and ERR of the regeneration medium increase with the increase in the number of channels because of the increase in the gas–solid heat transfer contact area. It is easy to cause a blockage if the number of channels is too large. Therefore, when selecting filler, the number of channels should be chosen so that a non-clogging filler chamber with a high filler module is formed. Figure 13 shows the effect of packing height on heat transfer efficiencies. The results in Figure 7 show that in the stable stage, the temperature distribution of gas and solids in approximately linear with the height of the regeneration module. It can be seen from Figure 13 that the heat transfer efficiency of the regeneration medium increases with the increase in filler height, which is consistent with the conclusion of You et al. [21].

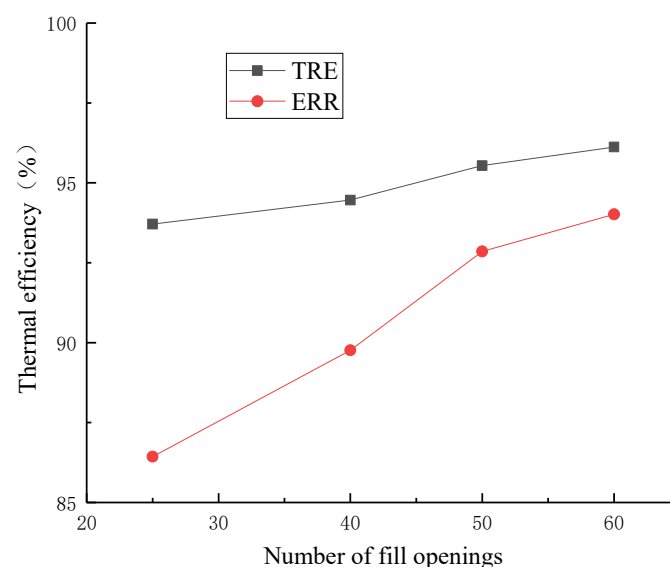


**Figure 12.** Effect of the numbers of regenerative media channels on heat transfer efficiencies.

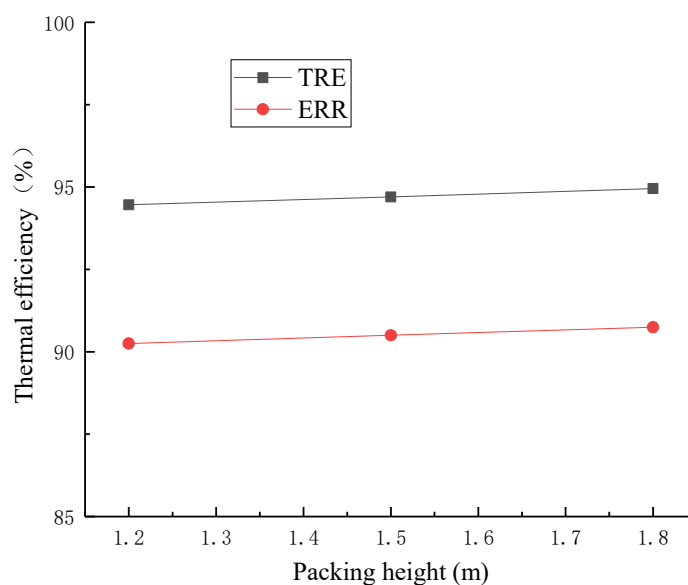


**Figure 13.** Effect of the packing height on heat transfer efficiencies.

#### 4.3.4. Effect of Regenerative Media Materials and the VOC Concentration

The honeycombs used in the preceding calculation cases are dense alumina honeycombs. If the dense cordierite is used, the TRE decreases from 94.46% to 87.89%, and the ERR decreases from 90.25% to 84.75% under the same working conditions. Dense cordierite honeycombs have a lower density, specific heat, and thermal conductivity than dense alumina honeycombs. Due to their high heat capacity, dense alumina honeycomb ceramics outperform dense cordierite in heat transfer. The calculation also shows that the TRE falls from 94.46% to 88.07%, and the ERR falls from 90.25% to 84.87% when the air specific gravity increases by 25%.

## 5. Conclusions

In this paper, the influence of key parameters on the heat transfer efficiency of RTO was studied by numerical simulation of fluid flow in canisters. The calculation model's validity is confirmed by comparing numerical results to experimental data. With the increase in outlet flue gas temperature, the preheating air temperature gradually decreases in a single cycle. The analysis of the change rules of RTO heat transfer efficiency reveals that increasing filler cross-sectional area and filler height increases heat transfer efficiency, resulting in an increase in equipment cost. If the equipment is not blocked, shorter valve switch time and higher regeneration medium unit density are helpful to improve the heat transfer efficiency. Unless the removal efficiency of VOC treatment is reduced, it is recommended to reduce the inlet and combustion temperatures.

**Author Contributions:** Conceptualization, G.P. and F.Y.; methodology, G.P.; data curation, X.L.; writing—G.P.; funding acquisition, F.Y. All authors have read and agreed to the published version of the manuscript.

**Funding:** This work has been financially supported by the National Natural Science Foundation of China (No. 11802105, 12172152) and the Jiangsu Key Laboratory of Advanced Food Manufacturing Equipment & Technology (FMZ202020).

**Institutional Review Board Statement:** Not applicable.

**Informed Consent Statement:** Not applicable.

**Data Availability Statement:** Not applicable.

**Acknowledgments:** The authors gratefully acknowledge the financial support from the National Natural Science Foundation of China (No. 11802105, 12172152).

**Conflicts of Interest:** The authors declare no conflict of interest.

## References

1. Tsuji, H.; Gupta, A.K.; Hasegawa, T.; Katsuki, M.; Kishimoto, K.; Morita, M. *High Temperature Air Combustion: From Energy Conservation to Pollution Reduction*; CRC Press: Boca Raton, FL, USA, 2002.
2. Lewandowski, D.A. *Design of Thermal Oxidation Systems for Volatile Organic Compounds*; CRC Press: Boca Raton, FL, USA, 2017; pp. 157–168.
3. Hao, X.; Li, R.; Wang, J.; Yang, X. Numerical simulation of a regenerative thermal oxidizer for volatile organic compounds treatment. *Environ. Eng. Res.* **2018**, *23*, 397–405. [[CrossRef](#)]
4. Giuntini, L.; Bertei, A.; Tortorelli, S.; Percivale, M.; Paoletti, E.; Nicoletta, C.; Galletti, C. Coupled CFD and 1-D dynamic modeling for the analysis of industrial Regenerative Thermal Oxidizers. *Chem. Eng. Process.* **2020**, *157*, 108117. [[CrossRef](#)]
5. Kang, K.; Hong, S.-K.; Noh, D.-S.; Ryou, H.-S. Heat transfer characteristics of a ceramic honeycomb regenerator for an oxy-fuel combustion furnace. *Appl. Therm. Eng.* **2014**, *70*, 494–500. [[CrossRef](#)]
6. Hong, S.K.; Noh, D.S.; Lee, E.K. Improvement in thermal efficiency of regenerator system by using oxy-fuel combustion. *Appl. Therm. Eng.* **2015**, *87*, 648–654. [[CrossRef](#)]
7. Gosiewski, K.; Pawlaczyk, A.; Jaschik, M. Energy recovery from ventilation air methane via reverse-flow reactors. *Energy* **2015**, *92*, 13–23. [[CrossRef](#)]
8. Gosiewski, K.; Pawlaczyk-Kurek, A. Aerodynamic CFD simulations of experimental and industrial thermal flow reversal reactors. *Chem. Eng. J.* **2019**, *373*, 1367–1379. [[CrossRef](#)]
9. Lin, C.-N.; Jang, J.-Y.; Lai, Y.-S. Two dimensional thermal-hydraulic analysis for a packed bed regenerator used in a reheating furnace. *Energies* **2016**, *9*, 995. [[CrossRef](#)]
10. Marín, P.; Díez, F.V.; Ordóñez, S. A new method for controlling the ignition state of a regenerative combustor using a heat storage device. *Appl. Energy* **2014**, *116*, 322–332. [[CrossRef](#)]
11. Marín, P.; Vega, A.; Díez, F.V.; Ordóñez, S. Control of regenerative catalytic oxidizers used in coal mine ventilation air methane exploitation. *Process Saf. Environ. Prot.* **2020**, *134*, 333–342. [[CrossRef](#)]
12. You, Y.; Huang, H.; Shao, G.; Hu, J.; Xu, X.; Luo, X. A three-dimensional numerical model of unsteady flow and heat transfer in ceramic honeycomb regenerator. *Appl. Therm. Eng.* **2016**, *108*, 1243–1250. [[CrossRef](#)]
13. You, Y.; Wu, Z.; Li, B.; Zhang, Z.; Pan, S.; Xu, X. 3D numerical simulation and optimization of honeycomb regenerators with parallel or crosswise arrangement of circular holes. *Chem. Eng. Process.* **2019**, *137*, 22–27. [[CrossRef](#)]
14. Yuan, F.; Wang, H.; Zhou, P.; Xu, A.; He, D. Heat transfer performances of honeycomb regenerators with square or hexagon cell opening. *Appl. Therm. Eng.* **2017**, *125*, 790–798. [[CrossRef](#)]
15. Alfarawi, S.; Al-Dadah, R.; Mahmoud, S. Transient investigation of mini-channel regenerative heat exchangers: Combined experimental and CFD approach. *Appl. Therm. Eng.* **2017**, *125*, 346–358. [[CrossRef](#)]
16. Lan, B.; Li, Y.-R. Numerical study on thermal oxidation of lean coal mine methane in a thermal flow-reversal reactor. *Chem. Eng. J.* **2018**, *351*, 922–929. [[CrossRef](#)]
17. Wang, F.; Lei, X.; Hao, X. Key factors in the volatile organic compounds treatment by regenerative thermal oxidizer. *J. Air Waste Manag. Assoc.* **2020**, *70*, 557–567. [[CrossRef](#)] [[PubMed](#)]
18. Gao, P.-F.; Gou, X.-L. Experimental research on the thermal oxidation of ventilation air methane in a thermal reverse flow reactor. *ACS Omega* **2019**, *4*, 14886–14894. [[CrossRef](#)] [[PubMed](#)]
19. Singh, G.; Kumar, G.; Murthy, D.S. Wavelet based simulation of thermal regenerator. *Therm. Sci. Eng. Prog.* **2019**, *9*, 142–147. [[CrossRef](#)]
20. Kumar, G.; Murthy, D.S. A multiresolution wavelet optimised finite-difference method for simulation of thermal regenerator. *Therm. Sci. Eng. Prog.* **2020**, *19*, 100669. [[CrossRef](#)]
21. You, Y.; Fan, A.; Lai, X.; Huang, S.; Liu, W. Experimental and numerical investigations of shell-side thermo-hydraulic performances for shell-and-tube heat exchanger with trefoil-hole baffles. *Appl. Therm. Eng.* **2013**, *50*, 950–956. [[CrossRef](#)]
22. You, Y.; Wu, Z.; Zeng, W.; Zhang, Z.; Wang, S.; Dai, F.; Yi, Z. CFD modeling of unsteady SCR deNOx coupled with regenerative heat transfer in honeycomb regenerators partly coated by Vanadium catalysts. *Chem. Eng. Res. Des.* **2019**, *150*, 234–245. [[CrossRef](#)]
23. Don, W.G.; Robert, H.P. *Perry's Chemical Engineers' Handbook*, 8th ed.; McGraw-Hill Education: New York, NY, USA, 2008.